Non-redundant odor coding by sister mitral cells revealed by light addressable glomeruli in the mouse

Ashesh K. Dhawale[1,2], **Akari Hagiwara**[3], **Upinder S. Bhalla**[2], **Venkatesh N. Murthy**[3,*], and **Dinu F. Albeanu**[1,*]

[1]Cold Spring Harbor Laboratory, One Bungtown Road, Cold Spring Harbor, NY, 11724

[2]National Centre for Biological Sciences, Tata Institute of Fundamental Research, Bellary Road, Bangalore, 560065, India

[3]Dept. of Molecular and Cellular Biology, and Center for Brain Science, Harvard University, 16 Divinity Ave, Cambridge, MA 02138

Abstract

Sensory inputs frequently converge on the brain in a spatially organized manner, often with overlapping inputs to multiple target neurons. Whether the responses of target neurons with common inputs become decorrelated depends on the contribution of local circuit interactions. We addressed this issue in the olfactory system using newly generated transgenic mice expressing channelrhodopsin-2 in all olfactory sensory neurons. By selectively stimulating individual glomeruli with light, we identified mitral/tufted (M/T) cells that receive common input (sister cells). Sister M/T cells had highly correlated responses to odors as measured by average spike rates, but their spike timing in relation to respiration was differentially altered. In contrast, non-sister M/T cells correlated poorly on both these measures. We suggest that sister M/T cells carry two different channels of information: average activity representing shared glomerular input, and phase-specific information that refines odor representations and is substantially independent for sister M/T cells.

Introduction

The responses of neurons within a sensory circuit depend on the interaction between direct input received from sensory afferents, lateral input from neurons within the same circuit, as well as feedback from other brain areas. In mammals, olfactory sensory neurons send their axons to the olfactory bulb (OB), where there is a characteristic physical layout of inputs at the glomerular layer[1]. Each glomerulus receives convergent afferents from a large number of olfactory sensory neurons (OSNs) expressing the same odorant receptor[2,3]. The principal neurons in the OB, the mitral and tufted (M/T) cells, typically have only one primary dendrite that projects to a single glomerulus. A few dozen M/T cells share input from the same parent glomerulus[1]. M/T cells also receive lateral GABAergic and dopaminergic inputs from a variety of interneurons in the glomerular and external plexiform layers[1], thus allowing them to sample information from several functionally diverse glomeruli.

To what extent is the output of M/T cells shaped by the input from the parent glomerulus versus lateral signals originating from other glomeruli in the bulb? Do M/T cells that have their primary dendrites in the same glomerulus – referred to as "sister" cells – carry redundant information about odors to higher brain centers? Progress in answering these important questions about redundancy and the topography of lateral connectivity has been slowed by the nature of odor representations at the input layer, and the anatomy of the bulb. Activating individual input elements (glomeruli) selectively is difficult because individual odors tend to activate distributed populations of glomeruli[4,5] and not all glomeruli can be activated even with a large palette of odors[6].

Here we describe the development of new tools to activate glomeruli optically, with high spatial and temporal precision. We engineered transgenic mouse lines that express the light-activated ion channel channelrhodopsin-2 (ChR2)[7] specifically in olfactory sensory neurons. Then, using a digital mirror device (DMD) to deliver patterned light stimulation onto the olfactory bulb in conjunction with extracellular recordings, we obtained the glomerular receptive field maps of individual M/T cells. By identifying the parent glomeruli, we were able to examine directly the similarity of odor responses of sister and non-sister M/T cells.

Results

We generated transgenic mice that express ChR2-EYFP in all mature olfactory sensory neurons using the olfactory marker protein (OMP) promoter, such that all glomeruli were light-sensitive (Fig. 1a). We characterized the olfactory receptor ChR2 mice (ORC) mice *in vitro* using acute brain slices and laser scanning photo-stimulation[8]. Whole-cell patch clamp recordings from mitral cells (Fig. 1b,c) showed reliable light-evoked currents only in response to photo-stimulation of the glomerular layer. These responses were blocked by ionotropic glutamate receptor antagonists CNQX and APV (Fig. 1b–d, N=5 cells). Furthermore, when stimulating at sub-glomerular inter-foci spacing (15 μm), excitatory currents (Fig. 1d) were obtained by stimulation of only a single glomerulus for each recorded cell (Fig. 1c). Fluorescent dye (Alexa 546) loaded into the recorded mitral cell confirmed that its apical dendrite projected to the same glomerulus whose stimulation evoked currents, as indicated by the circle in Fig. 1c (right panels). Increasing the stimulation intensity led to larger currents (Supplementary Fig. 1a), as well as spread of the hotspot to areas adjacent to the input glomerulus (Supplementary Fig. 1b), presumably due to activation of ChR2 in axons of passage. These experiments confirmed that activation of ChR2 in olfactory sensory axons within single glomeruli could depolarize their terminals effectively, causing glutamate release to activate postsynaptic neurons.

Identification of parent glomeruli of M/T cells *in vivo* by photostimulation

We adapted a digital micro-mirror device (DMD) from a commercial DLP projector (see Methods) to construct an instrument that allowed us to illuminate the olfactory bulb surface with arbitrary light patterns (at ~470 nm, see Methods) and photo-activate glomeruli *in vivo* (Fig. 2). We could therefore optically control neuronal activity at sub-glomerular resolution, with each pixel on the DMD corresponding to a ~5 μm spot on the bulb surface.

We simultaneously recorded M/T cell activity using tetrodes that were inserted 250–300 μm deep into the olfactory bulb of anesthetized ORC mice (see Methods). The surface of the bulb was tessellated into a square grid and each square pixel was illuminated sequentially by single focal spots of light in a pseudo-random spatial order (Fig. 2a). The stimulating light spots were of the same size, or smaller (20–75 μm) than the average mouse glomerulus (~75 μm)[6,9]. Light stimulation induced rapid and reliable changes in firing, peaking at 25–50 ms and lasting for 100 ms on average (Fig. 2a).

For each single unit (Fig. 2c, left panel) satisfying our selection criteria (see Methods), we constructed a two-dimensional light activation map (2DLAM) at subglomerular resolution (75 μm down to 20 μm) (Fig. 2c, center and right panels, see Methods). The light intensity was successively lowered until no light triggered activity was seen in any unit being recorded (down to intensities lower than 2 mW/mm^2). This ensured that we were operating in the regime of minimal glomerular activation (Fig. 2d) with negligible non-specific activation of axons of passage, as observed in acute slice experiments.

Since any given M/T cell in the adult mouse olfactory bulb receives excitatory inputs from only one glomerulus[1], we interpreted the hotspots to be parent glomeruli for the corresponding M/T cells. This was supported by the observation that reducing light levels led to a single hotspot on the 2DLAMs for all 40 units that were light responsive. In addition, the average size of the hotspot at the lowest intensity of stimulation (73.6 ± 3.9 μm, N=40) was comparable to the size of the average mouse glomerulus (74.2 ± 1.2 μm), as measured in OMP-synaptopHluorin (OMP-spH) mice[10] (572 glomeruli, 9 hemibulbs, Fig. 2e), in agreement with anatomical studies[9]. Further, taking advantage of YFP expression in glomeruli, we overlaid functional hotspots (N=9) obtained from light mapping onto multiphoton z-stack projections of images of YFP glomeruli taken in the same animal (see Methods). The hotspots co-localized well with anatomical glomeruli (Fig. 3a and Supplementary Fig. 2a) and the FWHM of the hotspots fitted within the anatomical boundaries of matching glomeruli (Fig. 3b). Furthermore, the jitter between the centroids of hotspots and anatomical glomeruli was significantly smaller than the corresponding glomerular widths (Fig. 3c, see Methods). The parent glomerulus for each isolated M/T unit was thus identified optically, just as it was done *in vitro*.

Glomeruli are generally laid out in a single row on the bulb surface, but occasionally they can be stacked on top of each other. Since it could affect the correct assignment of parent glomeruli to M/T units, we quantified the frequency of this over-stacking. Multiphoton z-stacks of ORC-M and OMP-spH glomeruli obtained via the same surgical configuration used for the physiology experiments showed that only ~6% of glomeruli overlapped on the dorsal surface (5.94 ± 0.45%, 558 glomeruli, 4 ORC-M hemibulbs and 6.02 ± 1.16%, 875 glomeruli, 7 OMP-spH hemibulbs, Fig. 3d,e and Supplementary Fig. 2b).

Identification of sister and non-sister M/T cells by light

Using tetrodes or dual-tetrodes[11], we recorded odor responses simultaneously from multiple M/T units with defined parent glomerular identities. On average, we were able to isolate ~4 single units per recording site. We compared all possible pairs of light responsive units obtained at each recording site (N=35 pairs) by taking the difference of 2DLAMs corresponding to each unit (Fig. 4a–d). In some pairs, the hotspots were clearly spatially separated (Fig. 4b), while in others they were overlapping (Fig. 4d). Thus, the units shown in Fig. 4b appeared to receive inputs from different neighboring glomeruli, whereas the pair plotted in Fig. 4d shared the same glomerular territory.

We needed an objective criterion to classify the recorded M/T units into `sister' cells or `non-sister' cells (Fig. 4e). For each pair, we calculated the Euclidean distance between the centers of the hotspots, normalized by the mean width (FWHM) of the two hotspots considered (Fig. 4f). Our results indicate that the size of glomeruli is equal to or larger than 1 FWHM of the functional hotspots (Fig. 2e, 3a–c). Therefore, pairs of M/T units whose parent glomeruli were placed less than one mean FWHM apart were classified as sisters, and the rest as non-sisters. Two distinct populations emerged (Fig. 3f), unambiguously separable by the FHWM criterion. Out of the 35 M/T pairs considered, 20 were found to be sisters. In a second strategy, we computed the correlation between the 2DLAMs for each M/T pair (Supplementary Fig. 3, see Supplementary Information); this approach yielded the same

results. The surprisingly high proportion of sister pairs is due to two factors: heterogeneity in light excitability of glomeruli and pre-selection bias to overcome the intrinsically low chance (20–30%) of recording sister pairs (see Supplementary Information). We conclude that the physical separation between 2DLAM hotspots can be used to determine which M/T units share input from the same parent glomerulus.

Odor response diversity in sister M/T cells

We next investigated the odor response properties of these M/T unit pairs to a set of 42 odor stimuli. M/T firing is often locked to respiration[12] (Fig. 5a,b), that is, M/T cells tend to spike preferentially at a particular phase of the respiratory cycle. In response to an odor, M/T cell firing rates can increase or decrease from resting values, and the timing of spikes in relation to respiration can be altered[13,14,15]. We divided each cycle of respiration into 5 bins and populated these bins with spikes (Fig. 5b,c). The resulting vector, referred to as the phase tuning curve, was obtained for each M/T unit separately for the air period and odor period, across many respiratory cycles (Fig. 5b,c), for all 42 odors. For example, the unit shown in Fig. 5a,b spiked reliably at the beginning and towards the end of the respiratory cycle during fresh air, but shifted its phase preference to a different point in the cycle, and underwent a reduction in firing rate once allyltiglate was presented (Fig. 5b, lower panel).

Responses to multiple odors were compared in simultaneously recorded sister M/T cells (Fig. 5c). In the example shown, p-anis aldehyde increased the firing rates of both units, with odor triggered spikes occurring at all phases of the respiratory cycle. For heptanal, however, the firing rate increased for unit 1 but was suppressed for unit 2. In response to 2-heptanone, although both units increased their firing rates, the phases of the respiratory cycle at which they predominantly spiked were different. Thus, we observed similarities and differences in the odor responses of sister M/T cells.

We next systematically analyzed the activity of both sister and non-sister M/T unit pairs, focusing in particular on changes in firing rate and phase tuning.

Odors induce correlated changes in the firing rate of sister M/T cells

For each M/T unit, we calculated the average change in firing rate upon odor presentation for all 42 stimuli, and constructed a firing rate based odor response spectrum (F-ORS, Fig. 6a,b, see Methods). Sister M/T units tended to be similar in their firing rate changes (Fig. 6a) as quantified by the Pearson correlation coefficient between the F-ORSs (0.68 ± 0.05, N=20, Fig. 6c,d). In contrast, the F-ORSs of non-sister pairs were diverse (Fig. 6b) and had lower correlations (0.23 ± 0.11, N=15, $p = 2.4 \times 10^{-4}$, two-sample unpaired t test, Fig. 6c,d). To obtain a measure of reliability for individual units across different trials, we split the odor repeats and calculated `self' F-ORS correlations, whose average value was $0.67 \pm 0.04$ (N=40). Sister pairs' F-ORS and `self' correlations were not significantly different ($p = 0.81$, also true when using matched number of trials, data not shown). However, as observed in the examples shown (Fig. 5c, heptanal and 2-heptanone; Fig. 6a, arrows), some odors did trigger different changes in the firing rates of sister cells.

Sister M/T cells are desynchronized by odors

For each M/T cell, we constructed phase tuning curves during Air and Odor (Fig. 7a) for all stimuli. As a measure of similarity, we computed the correlation coefficient between the phase tuning curves in Air and Odor periods for each stimulus. We termed this the phase response, analogous to a firing rate response. The phase responses for all 42 odors then yielded a phase odor response spectrum (P-ORS) (Fig. 7b) for each cell. For a given stimulus, a high value of the phase response (close to 1) would indicate that odor

presentation did not cause a substantial change in the phase tuning curve compared to the preceding air period.

How similar are phase responses for sister and non-sister pairs? We found that for sister pairs the average P-ORS correlation was only 0.18 ± 0.07 (N = 20, Fig. 7c), higher, but not significantly different from the average correlation for non-sister pairs (0.05 ± 0.06, N = 15, p = 0.16). These low correlation values were not due to lack of reproducibility of phase response spectra across trials, since `self' P-ORS correlation was 0.61 ± 0.05 (N = 40), significantly higher than both sister and non-sister P-ORS correlations ($p < 10^{-5}$ and $p < 10^{-7}$ respectively). Thus, unlike in the case of firing rate changes described above (Fig. 6), odors induce differential phase responses in sister as well as in non-sister M/T pairs.

How do odors induce distinct phase responses in sister cells – do they start with similar phase tuning curves that diverge upon odor stimulation, or do they start with different phase tuning curves even at rest (Air)? To determine the phase relationship between units, we calculated the correlation coefficient between the phase tuning curves of the two units of an M/T pair, for all stimuli used. We calculated this inter-unit phase similarity (PS) separately for Air and Odor periods (Fig. 7d). In both the example shown and over the entire population of sister M/T cells, the average phase similarity for all stimuli was high during Air, and was significantly reduced when odors were presented (Fig. 7d–f, Avg. $PS_{Air} = 0.45 \pm 0.02$, Avg. $PS_{Odor} = 0.27 \pm 0.02$, N=20 pairs times 42 odors, $p < 10^{-7}$, two-sample K-S test). This drop in phase similarity upon odor presentation was not due to a lack of reproducibility of phase tuning curves across trials since the `self' phase similarity was high in both Air and Odor conditions (Avg. `Self'-$PS_{Air} = 0.45 \pm 0.01$, Avg. `Self'-$PS_{Odor} = 0.45 \pm 0.01$, p = 0.05, two-sample K-S test, Fig. 7f). Non-sister pairs had a broad, poly-modal distribution of phase similarities at rest (Air), with modes at positive and negative similarity values (Fig. 7e), clearly different from the distribution of sister pairs (p = 0.004, two sample K-S test). This implies that different pairs of non-sister units fired consistently with different phase lags. Odor presentation flattened the distribution of phase similarity between the non-sister M/T units (Fig. 7e).

We obtained similar results if we focused on just the mean firing phase instead of the entire phase tuning curve for each stimulus (Supplementary Fig. 4 and Supplementary Information). We also examined the spiking relationship (Supplementary Fig. 5 and Supplementary Information) between pairs of M/T units using the more commonly-used spike time correlation analysis. This analysis indicated that odor presentation led to significant broadening of the peak and a drop in peak height of the M/T units' auto-correlograms, as well as of sister pairs' cross-correlograms (Supplementary Fig. 4a,c,d). Closer inspection revealed periodic modulation of spike timing in the beta and gamma frequency range for some M/T pairs, as described before[16] (Supplementary Fig. 6), but on average we did not detect significant power in these bands via coherence measurements at a population level (see Supplementary Information).

Odorants tend to activate multiple glomeruli. To investigate the effects of activating only the parent glomerulus on the phase properties of sister M/T pairs, we used the minimal light stimulation strategy (Figs. 2 and 4) to modulate activity of single glomeruli (see Methods), by presenting light pulses continuously for 200 ms periods. As expected, light activation of individual glomeruli significantly increased the firing rate of sister M/T units compared to baseline (Avg. 2.63 ± 0.47 Hz in Air versus 9.10 ± 0.72 Hz in Light period, p < 0.001 by two-sample paired t-test). The phase similarity between sister pairs was indistinguishable between Air and Light conditions (Avg. $PS_{Air} = 0.43 \pm 0.14$, Avg. PSLight = 0.42 ± 0.12, N=20 pairs, p=0.88 two-sample K-S test, Fig. 7g,h), even in instances when light stimulation changed the phase preference of the sister M/T units (Fig. 7g).

Data described in this section indicate that sister M/T units are entrained by respiration to fire synchronously at rest, but become desynchronized (in terms of their firing relation to respiration) by odors. However, light activation of just the parent glomerulus altered the phase properties of sister units in similar manner. Non-sister M/T units fire with consistent phase lags with respect to each other when at rest. Upon odor stimulation, these predictable phase relationships are also disrupted.

Odor induced firing rate and phase changes are independent

Are the differential firing rate and phase responses in sister M/T units (Figs. 6 and 7) we observed caused by the same odors? To answer this question, we identified odors that affected one unit in a distinct manner compared to the other (see Methods).

More odors had differential effects on phase than on firing rate in sister pairs (18.7 ± 3.0 % versus 9.3 ± 2.3 % of odors, p = 0.02, Wilcoxon signed-rank test, Fig. 8a), as anticipated from the data shown in Figs. 6 and 7. Importantly, the percentage overlap between odors that caused differential responses in firing rate and phase was 1.6 ± 0.6 %, not different from chance (1.4 ± 0.5 %; Fig. 8a, p = 0.68, by Wilcoxon signed rank test, and see Supplementary Information). For non-sister M/T pairs similar percentages of odors caused both firing rate and phase similarity changes ($19.1 \pm 3.9\%$ versus $18.1 \pm 5.4\%$), also overlapping only to chance levels (p = 0.95, Wilcoxon signed-rank test). It is noteworthy that similar percentage of odors caused a decrease in phase similarity for sister (18.1 ± 3.0 %) and non-sister pairs (19.1 ± 3.9 %, p = 0.51, two-sample K-S test).

These results demonstrate that odors can induce differential changes in the phase of sister M/T cells without inducing differential changes in firing rates. Therefore, changes in phase and firing rate are independent.

Discussion

We engineered transgenic mice with optically excitable glomeruli, which offer many possibilities for dissecting the circuitry of the early olfactory system. Here, we use them to identify sister M/T cells and demonstrate that their odor responses are not redundant.

Optical activation of inputs to the olfactory bulb

The expression of ChR2 in the OSNs provides unprecedented control over glomeruli, the elementary input units of the bulb. This is an important advance in the study of olfaction since it has been difficult to selectively activate every glomerulus in a region with odors. This approach could be extended to map the `surround' for each M/T neuron, uncovering glomeruli that provide inhibitory input, and thus obtain the `glomerular receptive field' for each M/T cell, which has not been possible until now[15]. Beyond circuit mapping, these mice could also be used for behavioral studies to test hypotheses about odor coding and perception[17,18].

The ORC mouse contrasts with the Thy1-ChR2 mouse[19], which expresses ChR2 in a large fraction of M/T cells. Light control of neuronal activity in these Thy-1 ChR2 mice bypasses the first level of processing, and is agnostic to important transformations on the inputs that take place in the glomerular layer, including feedforward inhibition[20,21]. The two transgenic lines are likely to provide complementary information on circuits in the olfactory bulb.

The DMD patterned illumination strategy adapted here, has been employed extensively in vision research[22], as well as to control neuronal activity in other systems[23]. In comparison to laser scanning photo-stimulation, DMDs can stimulate multiple foci in parallel to deliver a range of stimuli - from single spots to spatio-temporally complex natural (odor like) or even

arbitrary activity patterns. Finally, different stimulation wavelengths can be easily co-projected to trigger excitatory and inhibitory responses in parallel, for multi-color control of neuronal circuits[24,25].

Response properties of sister M/T cells: similarities and differences

In vivo studies using extracellular recordings in the olfactory bulbs of rodents came to divergent conclusions about the similarities in odor responses of neighboring M/T cells[26,27]. This was presumably because they could not tell apart sister from non-sister pairs, in contrast to our study. We found that sister cells were correlated in their firing rate changes. This is in line with the prevalent view that the glomerulus is homogenous in terms of receptor type innervation[3], therefore sister cells should receive common excitatory input. *In vitro* studies have provided evidence for strong coupling between the primary dendrites of sister mitral cells, through gap junctions[28, 29], or glutamate spillover[30, 31]. Slice experiments also suggest that activation of the olfactory nerve leads to highly correlated activation of sister M/T cells[32,21]. A recent *in vivo* study sequentially recorded from mouse mitral cells connected to the same glomerulus created by an ectopically expressed rat receptor. In line with our results, they found that M/T cell firing rate responses are correlated to each other, and additionally, mirror presynaptic activity in their parent glomerulus[33].

Correlated firing of principal cells in the olfactory bulb or its analog brain structures appears to be a common theme across species. In the antennal lobe of *Drosophila*, genetically identified homotypic projection neurons (PNs), the fly analogs of sister M/T cells, fired in synchrony at rest, and odor presentation triggered a further increase in spiking correlations[34]. In experiments on the tadpole olfactory bulb[35], imaging activity of large populations of M/T cells using calcium sensitive dyes identified clusters of highly similar M/T cells which were shown in some instances to be connected to the same glomerulus. Our observation that odors desynchronize pairs of sister M/T cells is at odds with these findings from other species. Possible reasons include the limited numbers of odors used in the above studies, an expanded role of local interneurons in sculpting bulbar activity patterns, and the active sampling of odors by sniffing in mammals.

It is important to stress that we presented different odorants at a single nominal liquid dilution (1:100, see Methods). It would be interesting to systematically explore the effect of odor concentration on the firing and phase properties we have catalogued, in a future study.

Origin of sister M/T cells' differential phase responses

Where and how does the non-redundancy in phase properties of sister M/T cells arise? One possibility is that OSNs innervating the same glomerulus are heterogeneous in their phase responses by virtue of their spatial positioning within the olfactory epithelium[36]. Per contra, differences in the timing of sensory axon inputs within a glomerulus have not been found[37]. Additionally, we did not observe a consistent phase relationship between sister units in terms of one cell systematically leading or lagging another (Supplementary Fig. 4 d,e), which would be expected if sister units received signals from spatially distinct groups of OSNs. Alternatively, differences in M/T cells intrinsic properties, such as varying spiking thresholds or differences in the expression and distribution of various ion channels, may account for the unpredictable effects of different odors on sister units. However, it is hard to envision any odor specific effects in these scenarios. Furthermore, using light stimuli to activate only the parent glomerulus of sister units produced coordinated modulation of the phase tuning curves of sister units (Fig. 7g,h). Therefore, it is unlikely that the differences in phase properties of M/T sisters observed upon odor stimulation are related to differences in intrinsic properties of the units. A circuit-level explanation seems more plausible. The phase of spiking may be influenced by the lateral input a M/T cell receives via interneurons in the

glomerular layer[20] and/or the granule cell layer[38]. The non-redundancy in odor responses of sister M/T cells could arise from the unique set of lateral `surround' input connections each cell receives. Since the numbers of odors that reduce phase similarities of sister as well as non-sister M/T pairs are comparable (Fig. 8a), we suggest that the surrounds of sister cells are as distinct as those of non-sister cells. In our model, common input and intraglomerular interactions dominate M/T spiking at rest, leading to sister cell synchronization. Surround inhibition becomes preeminent during odor presentation because of stronger overall input to the bulb. This leads to desynchronization of preferred spiking phase of sister M/T units and further alteration of phase relationships between non-sister units.

What are the mechanisms that can uncouple firing rate changes and phase changes? One possibility is that the excitatory sensory inputs drive the overall excitability of mitral cells, while lateral inhibition arrives at different times[39], even for sister M/T cells, to sculpt the pattern of firing (Fig. 8b). This requires that sister M/T cells receive synaptic inputs from different populations of interneurons, which is plausible but remains to be established.

Spike counts and spike timing are independent channels of information

A single sniff is sufficient for a rodent to distinguish closely related odors[40], thus the sniff has been thought of as representing a snapshot of the outside olfactory world. M/T cells can convey odor information to higher brain regions by modulation of either the number of spikes in each respiratory cycle, or the timing of these spikes within the cycle. The first strategy would be a form of a rate code, while the second would be a time code. Our finding that sister cells are similar with respect to firing rate changes but dissimilar with respect to the timing of their spikes suggests that both types of codes may be utilized in an independent manner. This implies that the M/T cells are capable of conveying different kinds of information by multiplexing rate and time codes in the same spike train.

What are these different kinds of information? Since the phase of spiking is probably influenced by the lateral input an M/T cell receives, one possibility is that the temporal code is a representation of the subset of glomeruli in the surround that are activated by the stimulus, while the rate code might convey the activity level of the OSNs projecting to the primary glomerulus.

In other words, the temporal code may represent cross-receptor relationships that frequently differ between odors activating the same odorant receptor, whereas the rate code may be more specific to activation levels of an individual receptor which is likely to scale similarly for all odors that activate the same receptor. These two codes are largely independent (Fig. 8 and Supplementary Fig. 9).

How do downstream circuits read out the different timing of spikes? Olfactory cortical neurons are very sensitive to timing of inputs coming from M/T cells, because of precisely timed feedforward inhibition[41,42]. Therefore, sister M/T cells with different spike times may activate different populations of neurons. Other downstream brain regions that are less sensitive to timing differences may act in a more integrative mode. It will be of interest to determine whether there are such differences in bulbar target areas such as the olfactory tubercle, anterior olfactory nucleus and even the amygdala.

The non-redundancy that we see in the temporal characteristics of sister M/T cell activity suggests that many more information output channels are leaving the olfactory bulb than the number of ORN types entering it. Such an expansion of outputs suggests that the bulb is not just a relay station. On the contrary, interesting computations occur here that may be important in extracting various features from the inputs and conveying them to the cortex.

Methods

Generating the olfactory receptor ChR2-EYFP (ORC) mice

Mice were engineered to express chanelrhodopsin-2 (ChR2) fused to enhanced yellow fluorescent protein (EYFP) in all mature OSNs under the control of a 12 KB fragment of the rat olfactory marker protein (OMP) gene promoter[43]. Two transgenic lines (#32, #33, or ORC-Vs) had expression restricted to the vomeronasal organ and accessory olfactory bulb (AOB). A third line (#20, or ORC-M, used for this study) expressed ChR2-EYFP in both the olfactory epithelium and the main olfactory bulb, as well as in the vomeronasal organ and AOB.

Subjects

We used a total of 89 adult ORC-M transgenic animals and 12 OMP-spH heterozygous mice (PD60 – PD400, 25–55g). Each animal was anesthetized with a cocktail of ketamine/ xylazine (initial dose of 60|6 mg/kg, IP), attached subsequently to an anesthesia pump (Harvard Apparatus, Pump 11 Plus) and thermo regulated with a heating pad (FST TR-200). Flow of the anesthetics cocktail was kept at 40–70 μl per hour throughout a typical 12–15 hours acute experiment. Low melting-point agarose (1.5%, Sigma, Type III) was poured in a thin layer above the bulb surface, after performing craniotomy and duratomy. Cortex buffer[44] was constantly circulated via a perfusion pump (ColePalmer Masterflex C/L) above the exposure. All animal procedures were performed according to guidelines of the US National Institutes of Health and were approved by the Institutional Animal Care and Use Committee at Cold Spring Harbor Laboratory.

Slice electrophysiology and light stimulation

We recorded intracellularly from mitral cells in 300 μm thick horizontal olfactory bulb slices from PD15–PD30 mice, in voltage clamp mode, holding the membrane potential at −70 mV. We used ~5MΩ impedance patch pipettes filled with internal solution containing cesium gluconate and Alexa 546 fluorescent dye. Laser scanning photo-stimulation[8] (DPSS Lasers, 3501–100, 354 nm, ~15 μm beam diameter at the specimen) through a 4× objective (Olympus, UPlanApo, NA 0.16) was used to determine the position of the parent glomerulus. An ultraviolet laser was utilized because it was already in operation in the experimental station for glutamate uncaging and we found that the broad excitation spectrum of ChR2 allowed for its excitation at 354 nm. Grids of 8×8, 8×16 or 16×16 stimulation foci were superimposed onto the slice, making sure that the glomerular layer was properly sampled. We typically used 0.1 – 40 mW laser power (measured at the back focal plane of the objective), 1 to 10 milliseconds of light stimulation and 15 to 150 μm inter-foci spacing. Each cell we recorded from was filled with Alexa 546 dye and imaged under 4× and 60× magnifications.

In vivo electrophysiology

We recorded mitral/tufted cell activity in the olfactory bulb using gold plated tetrodes[45]. Tetrodes were constructed by twisting together four 12.5 μm polyimide coated nichrome wires (Kanthal Palm Coast), and fusing their insulation using a heat gun. To increase single unit yield, we also employed clusters of eight electrodes[11]. These were made either by gluing together two tetrodes using Loctite 420, or by twisting together and heat-fusing eight nichrome wires. The tip of the tetrode was cut at an angle to make penetration into brain tissue easier, and each electrode was gold-plated to an impedance of 400–600 kΩ at 1 KHz. The electrodes were lowered into the bulb (Sutter MP-285) until they reached the dorsal mitral cell layer, characterized by the presence of multiple units with coordinated, rhythmic respiratory tuned activity at a depth of approximately 250–300 μm from the pial surface.

Electrophysiological signals were amplified 200 times (RHA1016, Intan Technolofies LLC), filtered (band pass, 300 to 5 KHz), and digitized at 32 KHz (PCI-6259, National Instruments). The respiratory cycle of the mouse was recorded using piezo-electric stress transducers (RadioShack buzzer or Kent Scientific TRN0028 piezo-electric stress sensor) placed under the animal, amplified via custom electronics, and digitized in parallel with the neural signals.

In vivo light stimulation

To activate individual glomeruli in ORC mice, we used a DLP projector (Optoma EP727 or EP774) with its color wheel removed, also inserting a blue filter (Edmund Industrial Optics NT52-532) in the emission path. One SLR photo lens (Nikor 50 mm, f/1.4, AF) was placed in front of the projector and coupled to an achromatic doublet (Thorlabs, AC508-150-A1, FL = 150 mm) positioned so as to project the stimulus image at infinity. A second SLR photo lens (Voigtländer, Nokton 35 mm FL, f/1.2) was then used to focus the image onto the bulb (Fig. 2a). One pixel of a projected image corresponded to 4 μm on the X-axis and 5 μm on the Y-axis. A dichroic mirror (Chroma 530dcxr, round, 2 inch diameter) was used to guide blue light to the tissue. To get a timestamp of the light stimulus, an LED (Luxeon V, Lumileds) was used as a photodiode, and placed it in the optical path after the first SLR lens. Two SLR lenses (the same Nokton 35 mmFL and a Nikkor 105 mm FL, f/2.0, AF, see Fig. 2a) coupled front to front, and appended to an emission filter (Chroma, HQ510LP) were used to image the olfactory bulb onto the CCD chip of a camera (Vosskuhler 1300-QF) with a pixel size of 10 μm. Light stimuli were generally square in shape and were presented for 200 ms within 500 ms trials.

Odor Stimulation

42 odorants[46] were diluted in mineral oil (1:100, typically), and loaded into a custom built odor delivery machine[6] (Supplementary Table 1). We used a photo-ionisation detector (PID, Aurora Scientific Inc., Canada) to determine the concentration of some of the odorants. Air was passed through Whatman filters soaked in pure odorants and subsequently diluted to calibrate the PID signals. The measured concentrations ranged between 0.1 to 2%. If at least two units displayed light triggered activity in the fine scale light mapping, the panel of odorants was serially presented to the mouse over 3 to 5 repetitions. Each trial consisted of 10 seconds of air followed by 5 or 10 seconds of odor exposure, and 5 seconds of air. An inter-trial interval of 10 or 15 seconds was instituted to prevent olfactory adaptation.

Spatial comparison of functional hostpots to anatomical glomeruli

Image projections from multiphoton z-stacks tessellating the bulb were stitched together using ImageJ. Blood vessel branching patterns were employed as landmarks for automated image registration using elastic deformations (bUnwarpJ[47]) between the multiphoton z-stack image projections and bright field images of the bulb surface. The 2DLAMs were registered first to the bright field images, and subsequently the overlay onto the multiphoton images was constructed.

Counting frequency of over-stacked glomeruli

The dorsal surface of ORC-M and OMP-spH hemibulbs was sampled systematically via multiphoton microscopy. For each field of view, z-stacks of the glomerular layer were obtained and the corresponding two dimensional (x-y) glomerular contours were drawn manually. Glomeruli sharing non-zero number of pixels in x-y were considered over-stacked.

Data processing

All offline analysis was carried out in MATLAB (Mathworks) and Igor Pro (Wavemetrics). Single units were identified by manual spike sorting using MClust (MClust-3.5, A. D. Redish et al). The sorting features used were the energy, peak height, peak to valley difference, and the first 2 principal components of the spike waveform. The inter-spike interval histogram was used to test for single unit isolation, imposing the criterion that the percentage of events separated by less than 2 ms should be below 1% of the total spike interval count, indicating a well-defined refractory period.

To check single unit cluster quality, we have employed Isolation Distance, a commonly used metric[48]. Three waveform parameters were used to compute the Isolation Distance: energy, peak-valley difference and the first principal component. More than 85% of the single unit clusters used have isolation distances exceeding 20, which is a standard threshold value used in recent literature[49,50], see Supplementary Fig. 7a.

Light mapping—2DLAMs were constructed by determining the average firing rate change between the stimulus and pre-stimulus periods for each spot in the grid. In these maps, each pixel represents the average change in firing rate during a 200 ms light stimulation period for the corresponding spot on the bulb surface (Fig. 2c, middle panel). A two-sample Kolmogorov-Smirnoff test was used to test whether the distribution of spike counts in the 200 ms light period across repeats was significantly different (p < 0.01) from the spike counts in the 200 ms pre-stimulus period across all trials and repeats. If a map contained at least one significant pixel, it was subjected to further analysis.

To determine the spatial extent of the light hotspots, we selected the 2DLAMs obtained at the lowest laser intensity which still modulated activity in the recorded units. These light maps were re-sampled at 1 micrometer resolution by interpolation (Fig. 2c, right panel) and the hotspots fitted with two dimensional Gaussians (Fig. 2e). The full width at half maximum (FWHM) of this 2D Gaussian fit was taken as the width of the hotspot.

Odor mapping—To quantify the magnitude of the response of a unit to a given odor, several metrics were used. First, the firing rate change (FR) induced upon odor presentation was determined for each of the 42 odors to build a firing rate based odor response spectrum (F-ORS), as described in Equation 1.

$$FR = \left(\frac{spikes_{odor}}{t_{odor}} \right) - \left(\frac{spikes_{air}}{t_{air}} \right)$$

Eq. 1

Second, to quantify changes in the cells' respiratory phase response characteristics (Fig. 4), all spikes were binned into 5 respiratory phase bins. Binning was done separately for the odor and preceding air periods, generating odor and air phase tuning curves (PTC) respectively displayed in terms of normalized spike counts (NSC, 0 to 1) versus phase bin. The phase response (PR) was then defined as the correlation coefficient between the air and odor (or light) phase tuning curves (Equation 2).

$$PR = corr\left(PTC_{air}, PTC_{odor} \right)$$

Eq. 2

The above metrics were calculated for each of the 42 odors to generate the corresponding phase odor response spectra (P-ORS) for each unit.

Phase similarity—This metric was used to measure similarity between the phase tuning curves of pairs of M/T cell units in both air and odor (or light) presentation periods. The Pearson correlation coefficient was calculated between the phase tuning curves of the two units for each odor (Equation 4). The same procedure was carried out on the phase tuning curves for the air period preceding odor presentation (Equation 3).

$$PS_{air} = corr \left(PTC_{unit1,air}, \ PTC_{unit2,air} \right)$$

<div align="right">Eq. 3</div>

$$PS_{odor} = corr \left(PTC_{unit1,odor}, \ PTC_{unit2,odor} \right)$$

<div align="right">Eq. 4</div>

Phase similarity values can vary from −1 to 1: pairs of units firing at very similar phase of respiration will have values close to 1, units that fire in opposite phases will have a value of −1 and units with no consistent relation will have values close to 0.

`Self' comparison analysis—To quantify trial to trial variability in spike responses of the M/T cells, we divided the odor presentation trials into two groups and applied the above mentioned metrics. This procedure gave an upper bound for measuring similarity across groups.

Detection of differential odor responses—Differential firing rate changes: Firing rate changes upon switching from Air to Odor for the two units of a pair were rescaled (FR_R) to span the same range. This range corresponded to a confidence interval spanning two standard deviations (σ) about the mean firing rate change (μ) of each unit.

$$FR_R = \frac{FR - (\mu_{FR} - 2 * \sigma_{FR})}{4 * \sigma_{FR}}$$

<div align="right">Eq. 5</div>

A standard deviation based range was chosen in order to avoid outlier biases given by the maximum and minimum firing rate changes. We then performed `self' analysis to compute the variability across trials for each unit.

We performed the same transformation on the `self' firing rates (FR_S):

$$Rescaled \ FR_s = \frac{FR_s - \left(\mu_{FR_s} - 2 * \sigma_{FR_s} \right)}{4 * \sigma_{FR_s}}$$

<div align="right">Eq. 6</div>

We used the fluctuation in firing rate changes from trial to trial to compute a signal threshold. The threshold was picked at two standard deviations of the `self' FR (FR_S) difference distribution. Any difference in rescaled firing rate changes between the two units exceeding this threshold was classified as a differential response.

$$|\Delta FR_R| > \left(2 * \sigma_{\Delta FR_s} \right) \dots\dots\dots\dots\dots \text{Differential Firing Response}$$

<div align="right">Eq. 7</div>

Differential phase similarities: The distribution of PS_{air} for each pair of units was used to compute a signal threshold. Like above, the threshold was at two standard deviations from the mean PS_{air}.

$$|PS_{odor} - \mu_{PS_{air}}| > \left(2 * \sigma_{PS_{air}}\right)\ldots\ldots\ldots\text{Differential phase similarity}$$

Eq. 8

Supplementary Material

Refer to Web version on PubMed Central for supplementary material.

Acknowledgments

References

1. Shepherd, GM. The Synaptic Organization of the Brain. Oxford University Press; New York: 1998.

2. Vassar R. Topographic organization of sensory projections to the olfactory bulb. Cell. 1994; 79:981–991. [PubMed: 8001145]

3. Mombaerts P. Axonal Wiring in the Mouse Olfactory System. Annu Rev Cell Dev Biol. 2006; 22:713–37. [PubMed: 17029582]

4. Stewart WB, Kauer JS, Shepherd GM. Functional organization of rat olfactory bulb analysed by the 2-deoxyglucose method. The Journal of Comparative Neurology. 1979; 185:715–734. [PubMed: 447878]

5. Rubin BD, Katz LC. Optical Imaging of Odorant Representations in the Mammalian Olfactory Bulb. Neuron. 1999; 23:499–511. [PubMed: 10433262]

6. Soucy ER, Albeanu DF, Fantana AL, Murthy VN, Meister M. Precision and diversity in an odor map on the olfactory bulb. Nat. Neurosci. 2009; 12:210–220. [PubMed: 19151709]

7. Boyden ES, Zhang F, Bamberg E, Nagel G, Deisseroth K. Millisecond-timescale, genetically targeted optical control of neural activity. Nat Neurosci. 2005; 8:1263–1268. [PubMed: 16116447]

8. Shepherd GMG, Pologruto TA, Svoboda K. Circuit analysis of experience-dependent plasticity in the developing rat barrel cortex. Neuron. 2003; 38:277–289. [PubMed: 12718861]

9. Royet JP, Souchier C, Jourdan F, Ploye H. Morphometric study of the glomerular population in the mouse olfactory bulb: numerical density and size distribution along the rostrocaudal axis. J Comp Neurol. 1988; 270:559–68. [PubMed: 3372747]

10. Bozza T, McGann JP, Mombaerts P, Wachowiak M. In vivo imaging of neuronal activity by targeted expression of a genetically encoded probe in the mouse. Neuron. 2004; 42:9–21. [PubMed: 15066261]

11. Hartwich K, Pollak T, Klausberger T. Distinct Firing Patterns of Identified Basket and Dendrite-Targeting Interneurons in the Prefrontal Cortex during Hippocampal Theta and Local Spindle Oscillations. J. Neurosci. 2009; 29:9563–9574. [PubMed: 19641119]

12. Macrides F, Chorover SL. Olfactory bulb units: activity correlated with inhalation cycles and odor quality. Science. 1972; 175:84–87. [PubMed: 5008584]

13. Meredith M. Patterned response to odor in mammalian olfactory bulb: the influence of intensity. J Neurophysiol. 1986; 56:572–597. [PubMed: 3537224]

14. Khan AG, Thattai M, Bhalla US. Odor representations in the rat olfactory bulb change smoothly with morphing stimuli. Neuron. 2008; 57:571–585. [PubMed: 18304486]

15. Fantana AL, Soucy ER, Meister M. Rat olfactory bulb mitral cells receive sparse glomerular inputs. Neuron. 2008; 59:802–814. [PubMed: 18786363]

16. Kashiwadani H, Sasaki YF, Uchida N, Mori K. Synchronized oscillatory discharges of mitral/tufted cells with different molecular receptive ranges in the rabbit olfactory bulb. J. Neurophysiol. 1999; 82:1786–1792. [PubMed: 10515968]

17. Mouly AM, Holley A. Perceptive properties of the multi-site electrical microstimulation of the olfactory bulb in the rat. Behav. Brain Res. 1986; 21:1–12. [PubMed: 3741592]

18. Monod B, Mouly AM, Vigouroux M, Holley A. An investigation of some temporal aspects of olfactory coding with the model of multi-site electrical stimulation of the olfactory bulb in the rat. Behav. Brain Res. 1989; 33:51–63. [PubMed: 2544198]

19. Arenkiel BR. In vivo light-induced activation of neural circuitry in transgenic mice expressing channelrhodopsin-2. Neuron. 2007; 54:205–218. [PubMed: 17442243]

20. Aungst JL. Centre-surround inhibition among olfactory bulb glomeruli. Nature. 2003; 426:623–629. [PubMed: 14668854]

21. Gire DH, Schoppa NE. Control of on/off glomerular signaling by a local GABAergic microcircuit in the olfactory bulb. J. Neurosci. 2009; 29:13454–13464. [PubMed: 19864558]

22. Engert F, Tao HW, Zhang LI, Poo M. Moving visual stimuli rapidly induce direction sensitivity of developing tectal neurons. Nature. 2002; 419:470–475. [PubMed: 12368854]

23. Guo ZV, Hart AC, Ramanathan S. Optical interrogation of neural circuits in Caenorhabditis elegans. Nat. Methods. 2009; 6:891–896. [PubMed: 19898486]

24. Zhang F. Multimodal fast optical interrogation of neural circuitry. Nature. 2007; 446:633–639. [PubMed: 17410168]

25. Han X, Boyden ES. Multiple-color optical activation, silencing, and desynchronization of neural activity, with single-spike temporal resolution. PLoS ONE. 2007; 2:e299. [PubMed: 17375185]

26. Buonviso N, Chaput MA. Response similarity to odors in olfactory bulb output cells presumed to be connected to the same glomerulus: electrophysiological study using simultaneous single-unit recordings. J Neurophysiol. 1990; 63:447–454. [PubMed: 2329354]

27. Egaña J, Aylwin M, Maldonado P. Odor response properties of neighboring mitral/tufted cells in the rat olfactory bulb. Neuroscience. 2005; 134:1069–1080. [PubMed: 15994017]

28. Christie JM. Connexin36 Mediates Spike Synchrony in Olfactory Bulb Glomeruli. Neuron. 2005; 46:761–772. [PubMed: 15924862]

29. Kosaka T, Kosaka K. Neuronal gap junctions between intraglomerular mitral/tufted cell dendrites in the mouse main olfactory bulb. Neuroscience Research. 2004; 49:373–378. [PubMed: 15236862]

30. Nicoll RA, Jahr CE. Self-excitation of olfactory bulb neurones. Nature. 1982; 296:441–444. [PubMed: 6278326]

31. Urban NN, Sakmann B. Reciprocal intraglomerular excitation and intra- and interglomerular lateral inhibition between mouse olfactory bulb mitral cells. J. Physiol. 2002; 542:355–67. [PubMed: 12122137]

32. Schoppa NE, Westbrook GL. Glomerulus-Specific Synchronization of Mitral Cells in the Olfactory Bulb. Neuron. 2001; 31:639–651. [PubMed: 11545722]

33. Tan J, Savigner A, Ma M, Luo M. Odor Information Processing by the Olfactory Bulb Analyzed in Gene-Targeted Mice. Neuron. 2010; 65:912–926. [PubMed: 20346765]

34. Kazama H, Wilson RI. Origins of correlated activity in an olfactory circuit. Nature Neuroscience. 2009; 12:1136–44.

35. Chen T, Lin B, Schild D. Odor coding by modules of coherent mitral/tufted cells in the vertebrate olfactory bulb. Proceedings of the National Academy of Sciences. 2009; 106:2401–2406.

36. Miyamichi K, Serizawa S, Kimura HM, Sakano H. Continuous and Overlapping Expression Domains of Odorant Receptor Genes in the Olfactory Epithelium Determine the Dorsal/Ventral Positioning of Glomeruli in the Olfactory Bulb. J. Neurosci. 2005; 25:3586–3592. [PubMed: 15814789]

37. Wachowiak M, Denk W, Friedrich RW. Functional organization of sensory input to the olfactory bulb glomerulus analyzed by two-photon calcium imaging. Proc. Natl. Acad. Sci. U.S.A. 2004; 101:9097–9102. [PubMed: 15184670]

38. Jahr CE, Nicoll RA. Dendrodendritic inhibition: demonstration with intracellular recording. Science. 1980; 207:1473–1475. [PubMed: 7361098]

39. Kapoor V, Urban NN. Glomerulus-specific, long-latency activity in the olfactory bulb granule cell network. J. Neurosci. 2006; 26:11709–11719. [PubMed: 17093092]

40. Uchida N, Mainen ZF. Speed and accuracy of olfactory discrimination in the rat. Nat Neurosci. 2003; 6:1224–1229. [PubMed: 14566341]

41. Luna VM, Schoppa NE. GABAergic circuits control input-spike coupling in the piriform cortex. J. Neurosci. 2008; 28:8851–8859. [PubMed: 18753387]

42. Poo C, Isaacson JS. Odor representations in olfactory cortex: "sparse" coding, global inhibition, and oscillations. Neuron. 2009; 62:850–861. [PubMed: 19555653]

43. Danciger E, Mettling C, Vidal M, Morris R, Margolis F. Olfactory marker protein gene: its structure and olfactory neuron-specific expression in transgenic mice. Proc. Natl. Acad. Sci. U.S.A. 1989; 86:8565–8569. [PubMed: 2701951]

44. Holtmaat AJGD. Transient and persistent dendritic spines in the neocortex in vivo. Neuron. 2005; 45:279–291. [PubMed: 15664179]

45. Gray CM, Maldonado PE, Wilson M, McNaughton B. Tetrodes markedly improve the reliability and yield of multiple single-unit isolation from multi-unit recordings in cat striate cortex. J. Neurosci. Methods. 1995; 63:43–54. [PubMed: 8788047]

46. Adams, D. The Hitchhiker's Guide to the Galaxy. Pan Books; London: 1979.

47. Carreras I. Consistent and Elastic Registration of Histological Sections Using Vector-Spline Regularization. Computer Vision Approaches to Medical Image Analysis. 2006; 95:85.

48. Schmitzer-Torbert N, Jackson J, Henze D, Harris K, Redish A. Quantitative measures of cluster quality for use in extracellular recordings. Neuroscience. 2005; 131:1–11. [PubMed: 15680687]

49. Sigurdsson T, Stark KL, Karayiorgou M, Gogos JA, Gordon JA. Impaired hippocampal prefrontal synchrony in a genetic mouse model of schizophrenia. Nature. 2010; 464:763–767. [PubMed: 20360742]

50. Quirk MC, Sosulski DL, Feierstein CE, Uchida N, Mainen ZF. A Defined Network of Fast-Spiking Interneurons in Orbitofrontal Cortex: Responses to Behavioral Contingencies and Ketamine Administration. Front Syst Neurosci. 3
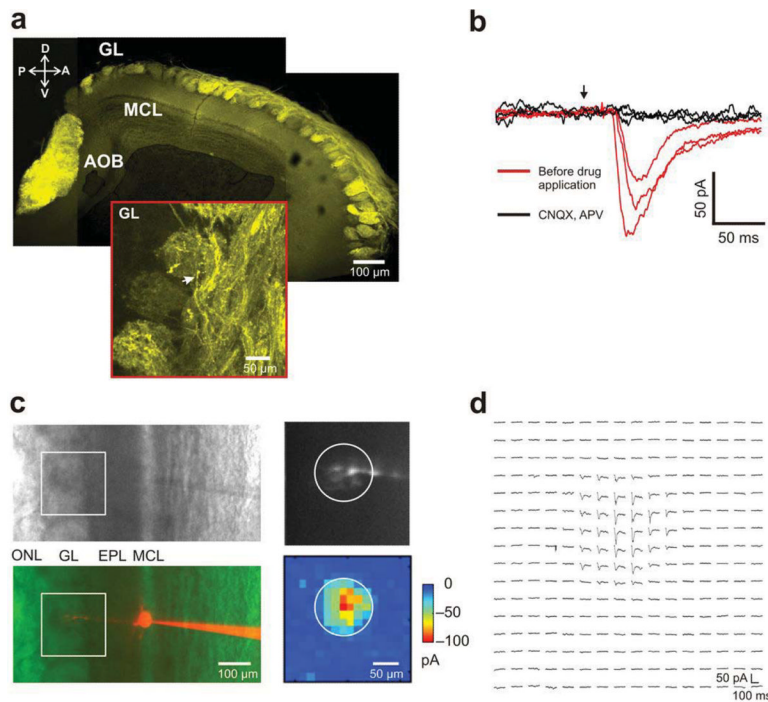
Figure 1. OMP-ChR2 (ORC) transgenic expression pattern; Laser scanning photo-stimulation (LSPS) identifies parent glomeruli for mitral cells in ORC mice olfactory bulb slices
a. Confocal micrograph of olfactory bulb sagittal section from ORC mice showing EYFP fluorescence; GL – glomerular layer, MCL – mitral cell body layer, AOB – accessory olfactory bulb, A-anterior, P-posterior, D-dorsal, V-ventral; scale bar is 100 µm. (*Inset*) higher magnification view: arrow indicates olfactory sensory neuron axons; scale bar is 50 µm.
b. Bath application of glutamate receptor antagonists CNQX and APV; the three traces for each of the conditions correspond to three adjacent photo-stimulation foci 50 µm apart; red trace – before drug application; black trace – during drug application; arrow indicates the time of photo-stimulation.
c. Phase (*Top left*) and red fluorescence image (*Bottom left*) of one mitral cell filled with Alexa 546; box indicates the field of photo-stimulation; (*Top right*) Primary dendrite and tuft projecting to a glomerulus. (*Bottom right*) Matching two-dimensional light activation map (16 X16 2DLAM); inter-foci distance = 15 µm; photostimulation duration = 1 ms. Note the fiduciary circle on the two panels. Color represents peak amplitude of the light induced currents; ONL – olfactory nerve layer; scale bar is 100 µm.
d. Currents recorded in the mitral cell by LSPS in **c** are shown at locations corresponding to each point in the 16 × 16 grid; traces were averaged across 4 repeats; 1.6 mW laser power was used. Scale bars are 50 pA and 100 ms respectively.
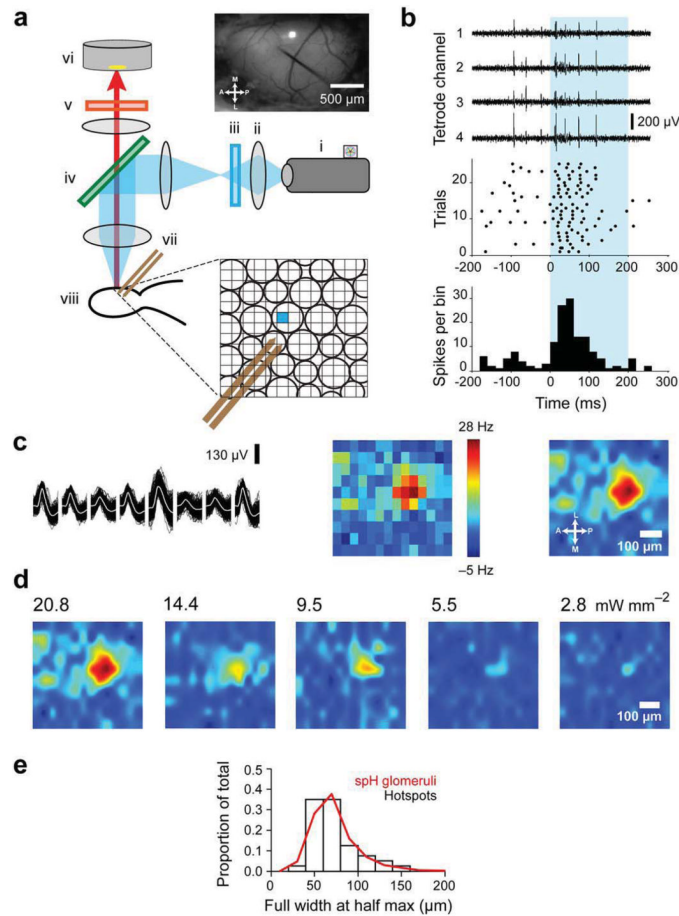
Figure 2. DMD patterned illumination in ORC mice maps the parent glomeruli of M/T cells *in vivo*

a. (*Left*) Schematics of DLP projector based photostimulation setup (*Top panel right*) Dorsal surface of the bulb with a tetrode positioned in the mitral cell layer. One square light spot can be seen projected onto the bulb surface; scale bar, 500 microns. (*Inset*) Cartoon schematic of glomeruli showing a sub-glomerular size light spot and dual-tetrodes positioned in the mitral cell layer. *i.* DLP projector *ii.* focusing lens, *iii.* blue excitation filter, *iv.* dichroic mirror, *v.* emission filter, *vi.* CCD camera, *vii.* dual-tetrode, *viii.* olfactory bulb.

b. (*Top*) Raw voltage traces corresponding to the four channels of a tetrode during photostimulation. (*Center*) Raster plot of spikes from an isolated single unit; (*Bottom*) Peri-stimulus time histogram (PSTH) with 25 ms time bins.

c. (*Left*) Example spike waveform of a single unit across the eight channels of a dual-tetrode. Dark traces - individual spikes; white line - average waveform. (*Center*) 2DLAM showing the change in firing rate of the M/T unit during photostimulation over 10 repeats; scale bar, 100 μm; light spot size, 50 μm. (*Right*) 2DLAM re-sampled by interpolation.

d. 2DLAMs obtained at different stimulation intensities (spot size, 50 μm). All maps were normalized to the highest bin in the 20.8 mW/mm^2 2DLAM.

e. Distribution of 2DLAM hotspot widths (FWHM) for all units (N = 40) obtained in a minimal photo-stimulation regime (black bars). Distribution of synaptopHluorin labeled glomerular widths (FWHM) from OMP-spH mice (Red line, N=572).
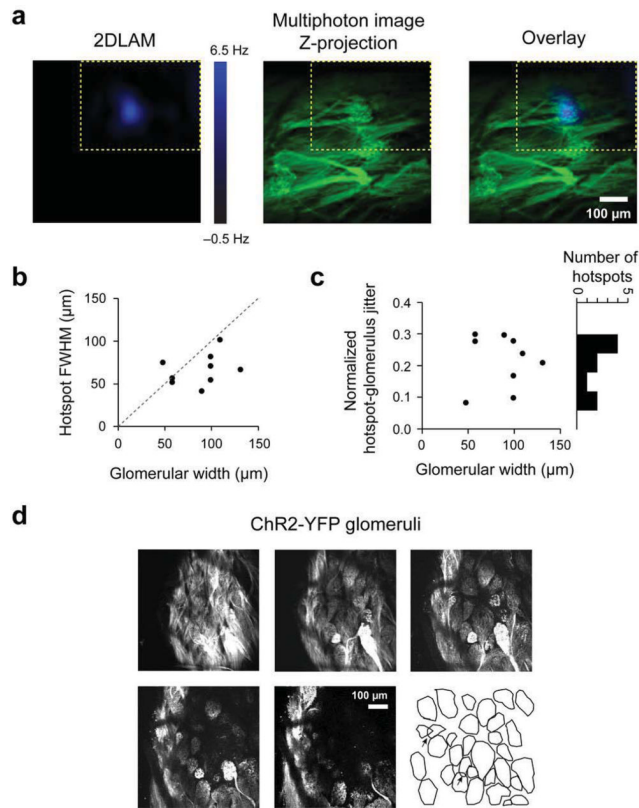
Figure 3. Functional hotspots correspond to anatomically identified glomeruli
a. (*Left*) Functional hotspot from representative two dimensional light activated map (2DLAM); (*Center*) Z-stack image projection of anatomical glomeruli from the same field of view as the 2DLAM obtained via multiphoton microscopy. (*Right*) Overlay of the 2DLAM and the z-projection. Yellow dotted lines indicate the boundaries of the 2DLAM.
b. Hotspot FWHMs plotted against corresponding anatomical glomerular widths.
c. Normalized spatial jitter between the centroids of functional hotspots and the corresponding anatomical glomeruli plotted against anatomical glomerular widths. The spatial jitter was normalized by the mean width of the anatomical glomerulus and the hotspot (a value of 1 corresponds to jitter of 1 glomerular width).
d. Example z-stack image projections of OMP-ChR2-YFP glomeruli obtained via multiphoton microscopy. Each image shown is a 20 μm thick projection, taken 20 μm apart in the z-axis from the subsequent one. Drawing illustrates contours of the glomeruli in the field of view. Arrows indicate overstacked glomeruli.
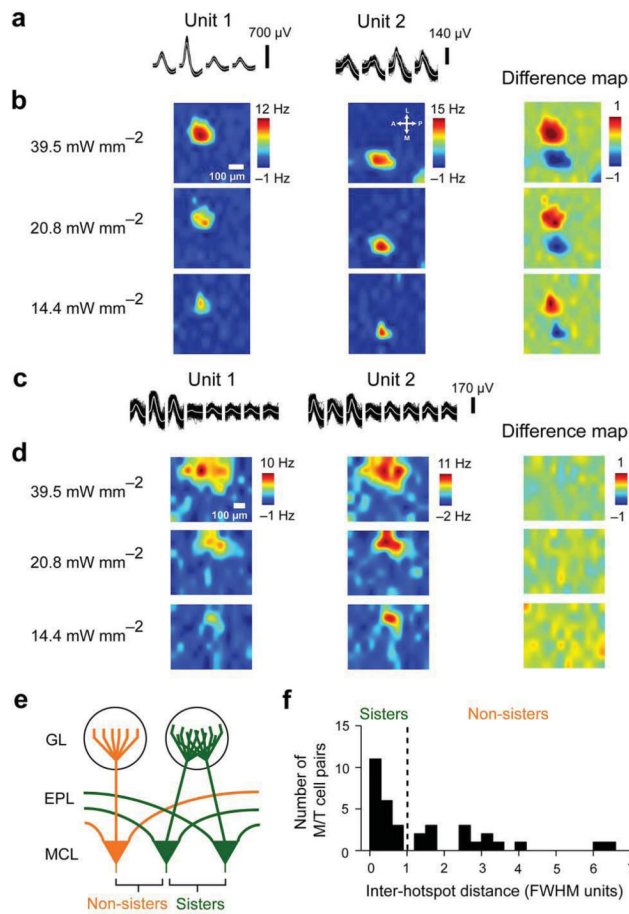
Figure 4. Light mapping sorts M/T cells into sister and non-sister pairs
a. Example spike waveforms on individual tetrode channels for two isolated non-sister M/T cell units.
b. 2DLAMs for the units shown in **A** at different light intensities used for stimulation. The color scale bar range to the right of the highest intensity maps indicates the range of firing rate changes with respect to baseline. All light maps for a particular unit are scaled to this range. Difference map refers to the difference between the normalized 2DLAMs of the two units, plotted for each of light intensities used; spatial scale bar is 100 μm.
c. Example waveforms for two isolated sister M/T cell units.
d. 2DLAMs for the units shown in **c** at different light intensities used for photo-stimulation. Color scale bar range, as described in **b**; spatial scale bar is 100 μm.
e. Cartoon schematic of parent glomerular connectivity for sister and non-sister M/T cells.
f. Separation of M/T cells into sisters and non-sisters based on Euclidean distance between the centers of light hotspots on 2DLAMs obtained in a minimal photo-stimulation regime. The distance between the centers of hotspots is expressed in units of the mean full width at half maximum (FWHM) of Gaussian fits to the two hotspots for each pair. Dotted line marks the separation between sister and non-sisters M/T cells and is placed at 1 FWHM.
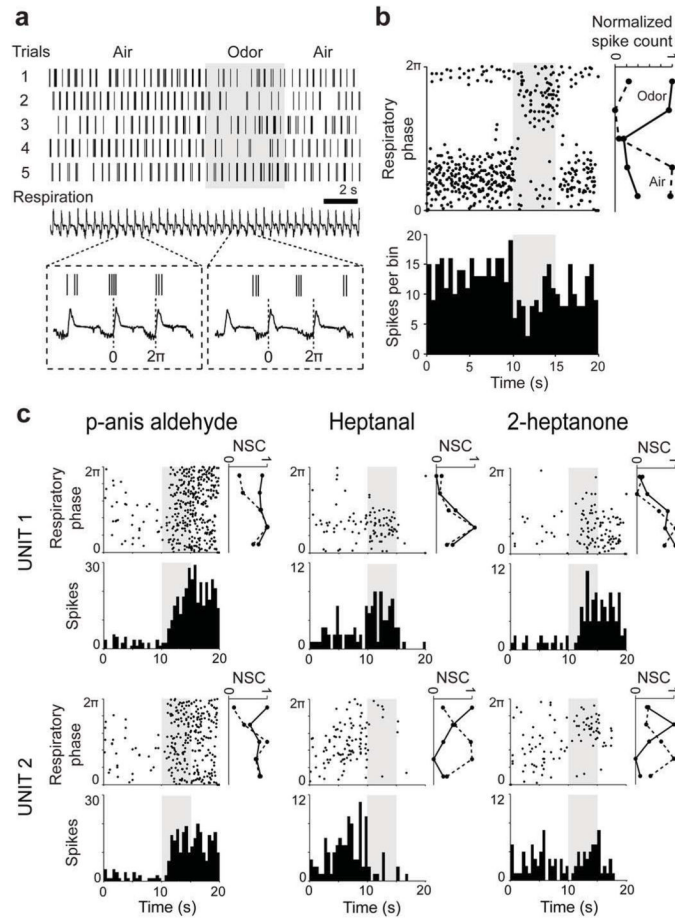
Figure 5. Examples of similarities and differences in odor responses of sister M/T cells
a. Example odor response of an M/T unit. (*Top*) Five odor stimulation trials are shown for this unit; vertical lines mark the time of a spike occurrence. Shadowed area indicates odor presentation window (5 s). (*Bottom*) Respiration trace. One respiratory cycle (labeled 0 to 2π) was typically ~500 ms long. *Inset:* expanded traces showing three respiratory cycles during air and odor presentation periods for one trial.
b. (*Top*) Phase-time plot of the odor response of the same M/T unit in **a**, shown over five repeats of allyl tiglate. Note the change in the preferred phase during odor stimulation (shadowed area). On the right of the phase-time plot are shown the phase tuning curves calculated during air (dotted line) and odor (continuous line) presentation where each respiratory cycle was divided into 5 time bins. (*Bottom*) PSTH of the same unit showing a drop in firing rate triggered by odor onset; bin width, 500 ms; NSC- normalized spike count.
c. Example odor responses to p-anis aldehyde, heptanal and 2-heptanone for two sister M/T cells (Unit 1 and Unit 2) shown as phase plots, PSTHs and phase tuning curves as in **b**. (*Left*) note the strong increase in firing, spread across all respiration cycle phases for both units; (*Center*) note the excitatory versus inhibitory response triggered by odor onset in the two units; (*Right*) note the change in preferred phase of Unit 2 triggered by the odor onset.
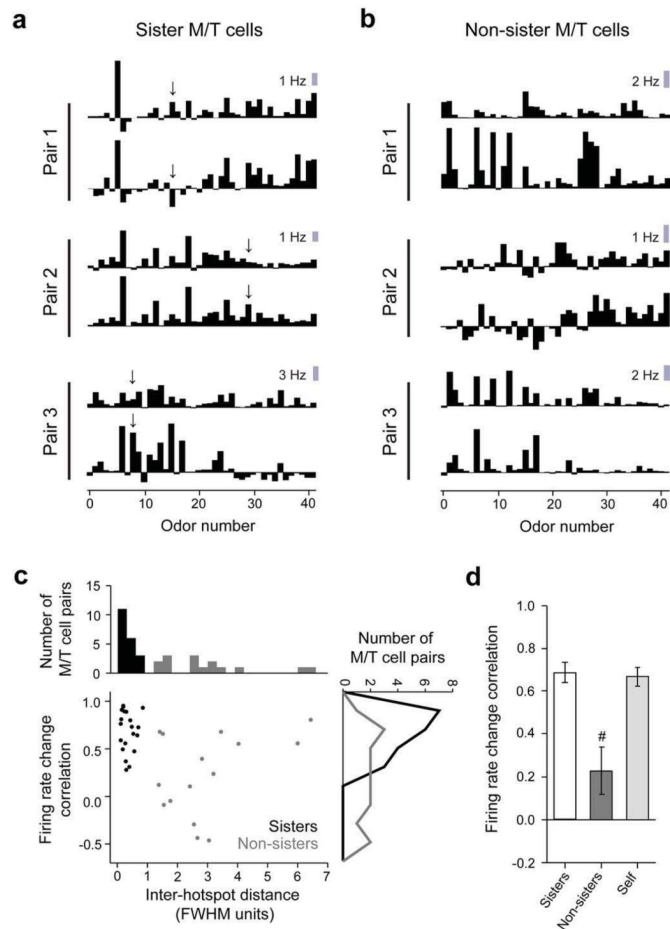
Figure 6. Sister M/T cells have correlated changes in odor induced firing rates
a. and **b.** Examples of firing rate odor response spectra (F-ORS) obtained using a set of 42
odors for three pairs of sister (**a**) and three pairs of non-sister M/T cells (**b**). Arrows in **a**
denote differential responses across pairs of sister units.
c. A scatter plot of the similarity (correlation coefficient) of odor-induced firing rate change
against the Euclidean distance between the centers of the hotspots in the 2DLAMs for each
pair of M/T units considered. Gray indicates non-sister M/T cells; black indicates sister M/T
cells. The marginal distributions are shown as histograms on the top and right axes. (*Top*)
Separation of units into sister and non-sister M/T cells, as shown in Fig. 3f. (*Right*)
Histograms of sister (N = 20) and non-sister pairs (N = 15) F-ORS correlations.
d. Average F-ORS correlations for sister and non-sister M/T cells; `self' refers to the same
unit (N = 40) probed across different blocks of odor repeats by splitting the total number of
trials in two; # marks $p < 0.05$ for F-ORS correlations, across groups with respect to sister
M/T pairs (e.g. sister versus non-sister M/T units). Error bars represent standard error of the
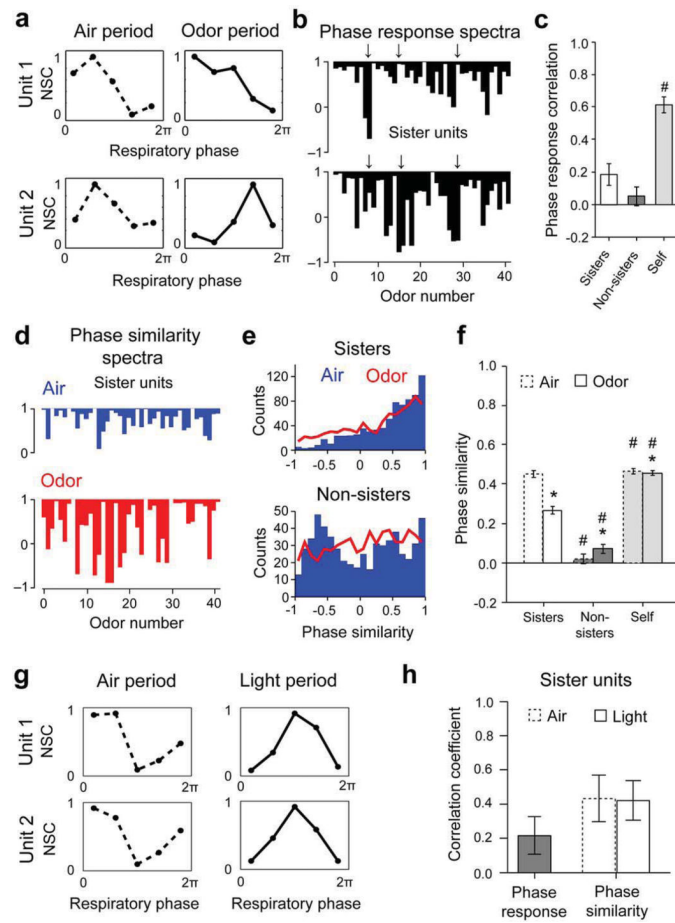mean (s.e.m.).

Figure 7. Odors disrupt phase correlations of sister and non-sister M/T cells

a. Example phase tuning curves for two M/T units (Unit 1 and Unit 2) during Air and Odor.

b. Phase response spectra for one representative sister M/T unit pair. Arrows indicate example mismatches between the spectra.

c. Average phase response spectra correlations between sister and non-sister M/T pairs.

d. Example phase similarity spectra for two sister M/T cells during Air (blue) and Odor (red) for 42 stimuli.

e. Histograms of phase similarity during Air (blue) and Odor (red) for all sister (N = 20) (*Top*) and non-sister (N = 15) (*Bottom*) M/T unit pairs for 42 stimuli.

f. Average phase similarity for sister and non-sister M/T pairs.

g. Example phase tuning curves for two M/T units (Unit 1 and Unit 2, different from panel **a**) during Air and Light activation of single parent glomeruli. Note that light induces similar changes in phase for both units.

h. (*Left*) Average phase response between Air and Light for individual sister M/T units; (*Right*) Average phase similarity between sister M/T pairs during Air (dotted line) and Light (continuous line).

`self' refers to similarity between phase tuning curves generated from the same unit, by splitting the number of trials into two; * $p < 0.05$ for comparisons within the same group (sister or non-sister M/T units) across conditions (Odor vs. Air); # $p < 0.05$ for same condition (Air or Odor), across groups (sister versus non-sister M/T units) with respect to sister M/T pairs.
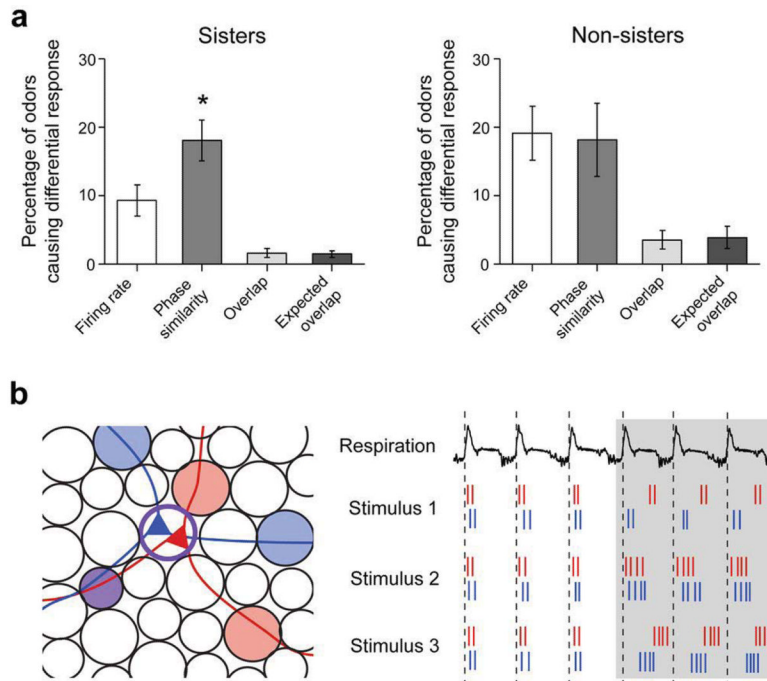
Figure 8. Odors trigger firing rate and phase changes in an independent manner
a. Average number of odors that induced differential responses in units of the same pair, considered in terms of firing rate changes or phase similarity; `overlap' refers to number of odors that induced significant differential changes in both firing rate and phase between units; `expected overlap' refers to the number of odors that would induce significant differential changes in both firing rate and phase, if the two were independent. Data is shown for sister (*Left*) and non-sister (*Right*) M/T pairs; * marks p < 0.05.
b. (*Left*) Cartoon representation of the diversity of sister M/T cell surround fields. (*Right*) Example spike trains of two model sister M/T cells (red and blue) during Air and Odor periods with respect to the respiratory cycle (top trace); Stimulus 1 elicits different phase shifts between the two neurons, but their firing rates are unchanged. Stimulus 2 elicits similar firing rate changes in both neurons, and their firing times remain correlated. Stimulus 3 elicits the same firing rate change in both neurons, but different phase shifts.